


Quasiparticle random-phase approximation in valence spaces: The case of magnetic dipole transitions

M. Frosini

*CEA, DES, IRESNE, DER, SPRC, LEPh, 13115 Saint-Paul-lez-Durance, France*W. Ryssens *Institut d'Astronomie et d'Astrophysique, Université Libre de Bruxelles, CP-226, 1050 Brussels, Belgium*K. Sieja **Université de Strasbourg, IPHC, France
and CNRS, UMR7178, 67037 Strasbourg, France*

(Received 10 January 2024; revised 13 May 2024; accepted 21 June 2024; published 2 July 2024)

Background: The low-energy enhancement observed recently in the deexcitation γ -ray strength functions, suggested to arise due to the magnetic dipole ($M1$) radiation, motivates theoretical efforts to improve the description of $M1$ strength in available nuclear structure models. Reliable theoretical predictions of nuclear dipole excitations are of interest for different nuclear applications and in particular for nuclear astrophysics, where the calculations of radiative capture cross sections often resort to theoretical γ strength functions. The quasiparticle random-phase approximation (QRPA) approach is arguably the most widely spread microscopic tool in this context since it can be applied to heavy nuclei and at the scale of the entire chart.

Purpose: We aim to benchmark the performance of QRPA calculations with respect to $M1$ γ strength functions, with a special emphasis on the description of the low-energy effects observed in the deexcitation strength.

Methods: We investigate the zero-temperature and finite-temperature (FT) magnetic dipole strength functions computed within the QRPA and compare them to those obtained from exact diagonalizations of the same Hamiltonian in restricted orbital spaces. Our sample consists of 25 spherical and deformed nuclei, with masses ranging from $A = 26$ to $A = 136$, for which the exact diagonalization of the respective effective Hamiltonian in three different valence spaces remains feasible.

Results: We find a reasonable agreement for the total photoabsorption strengths between both many-body methods but show that the QRPA distributions are shown to be systematically shifted down in energy with respect to exact results. Photoemission strengths obtained within the FT-QRPA formalism appear insufficient to explain the low-energy enhancement of the $M1$ strength functions evidenced by the exact diagonalization approach.

Conclusions: We ascribe the problems encountered in the zero- and finite-temperature QRPA calculations to the lack of correlations in the nuclear ground state and to the truncation of the many-body space. In particular, the latter prevents obtaining the sufficiently high level density to produce the low-energy enhancement of the $M1$ strength function, making the (FT-)QRPA approach unsuitable for predictions of such effects across the nuclear chart.

DOI: [10.1103/PhysRevC.110.014307](https://doi.org/10.1103/PhysRevC.110.014307)

I. INTRODUCTION

Radiative neutron capture plays a crucial role in many applications of nuclear physics, from reactor design to astrophysical simulations. Experiments cannot realistically obtain the cross section of this process in all relevant conditions or even for all relevant nuclei; in the case of r -process nucleosynthesis thousands of extremely exotic nuclei far beyond the reach of current accelerators are involved [1]. Reaction theory can provide the missing information through the statistical

Hauser-Feshbach model, but the resulting cross section depends strongly on the structure of the compound nucleus formed and in particular on its probability to deexcite through the emission of a γ ray [2]. This probability is characterized by the γ -ray strength function of the nucleus, a quantity that should ideally be predicted reliably across the entire nuclear chart by nuclear structure models.

Although radiation of all multipolarities can contribute to the strength function, the main contributions to neutron capture cross sections are due to dipole radiation: both the giant electric dipole resonance at high energy and the magnetic spin-flip resonance at low energy. Traditionally, dipole

*Contact author: kamila.sieja@iphc.cnrs.fr

strength. functions were modeled in the fully phenomenological Lorentzian approximations [3,4]. However, important deviations from statistical behavior were evidenced at low γ -ray energies, in particular the so-called low-energy enhancement (LEE) of the dipole strength [5–10]. Such an enhancement, if present in neutron-rich nuclei, could increase the neutron-capture cross sections up to a 100 times [10], depending on whether the electric or magnetic dipole strength is largest.

Significant theoretical effort was devoted in recent years to explain the LEE. The authors of Ref. [11] achieved an initial breakthrough: For the first time, the deexcitation strength function was obtained from interacting shell-model (SM) calculations, pointing to the magnetic-dipole character of the LEE. Further SM calculations of both the $M1$ and $E1$ dipole strength functions of ^{44}Sc confirmed the magnetic-dipole nature [12] of the LEE and predicted a flat behavior of the $E1$ strength functions towards zero γ -ray energy. Further SM studies addressed the LEE more systematically and concluded that the enhancement is produced by the low-energy γ rays coming from the quasicontinuum of nuclear states [13–18].

Other studies of the LEE so far have been based on the (quasiparticle) random-phase approximation or (Q)RPA but typically generalize the traditional QRPA formalism by including, for instance, the effect of finite temperature. Two early studies were limited to the electric dipole strength function [19,20], while a more recent study addressed both dipole modes in ^{56}Fe [21]. The combined deexcitation strength of $E1$ and $M1$ obtained by the authors of the latter appeared insufficient to describe the low-energy data from Oslo experiments [5], while shell-model calculations achieved good agreement with only the magnetic decay strength [22].

The interacting shell model with highly tuned empirical Hamiltonians is known to provide precise results for spectroscopy and electromagnetic transitions. Unfortunately due to computational complexity its applications are still restricted to particular regions of nuclei. The necessity of deriving a suitable effective interaction for each model space adds to the already complicated task of the complete diagonalization of the many-body Hamiltonian, making it impossible to achieve systematic studies that span the nuclear chart. The (quasiparticle) random-phase approximation or (Q)RPA approach provides an interesting alternative: This method scales polynomially with particle number thanks to a truncation of the many-body space to either two quasiparticle excitations (QRPA) or particle-hole excitations (RPA) of a mean-field reference state. Because of this favorable scaling, (Q)RPA and its extensions [23] have been widely used in many different contexts [24], from *ab initio* interactions to systematic studies across the nuclear chart with energy density functionals (EDF) [25–27].

However, the truncation of the many-body space of (Q)RPA necessarily misses physical effects present in a complete SM calculation such as the LEE. More advanced many-body approaches aim to decrease such errors by including higher-order excitations [two-particle two-hole (2p-2h), 3p-3h, phonon-coupling], which enhances the fragmentation of the spectrum while shifting the centroid of the resonance

[28–32]. However, such calculations are generally very demanding and are impractical for global application. A more pragmatic approach to provide a complete set of dipole γ -ray strength functions derived from QRPA calculations was developed in Refs. [26,33,34] by adding further empirical corrections to account for the missing correlations and to reproduce the available data. Reference [35] in particular provided a complete set of dipole strength functions that include low-energy structure effects by phenomenological corrections inspired by SM calculations. Such a treatment appeared successful but surely is far from being satisfying if one aims at a fully coherent microscopic description of strength functions across the nuclear chart: A limited number of available shell-model results does not guarantee the universality of the observed low-energy effects which, if applied globally through a phenomenological recipe, may introduce unrealistic behaviors of the neutron-capture cross sections for exotic nuclei. On the flip side, $M1$ strengths have been suggested repeatedly as an excellent candidate observable to constrain future EDF parametrizations since they are sensitive to the spin-isospin channel [36–41].

Although SM calculations cannot cover sizable portions of the nuclear chart, their exact nature is the ideal benchmark of approximate methods that scale more gently such as the QRPA [35,42]. Our goal here is to understand in more detail the deficiencies of the QRPA approach: We study the differences between strength functions obtained with exact diagonalization and QRPA calculations in identical model spaces and employing identical SM Hamiltonians. Reference [43] constitutes a previous benchmark along this line: The authors studied a number of transition operators (Gamow-Teller, spin-flip, and quadrupole) but limited themselves to a few nuclei in the *sd* and *pf* shells and RPA calculations that did not include the effects of pairing. Here we concentrate on the magnetic dipole operator, include the effect of pairing by utilizing the QRPA and cover a wider range of nuclei, with masses from $A = 20$ to 136, in three distinct model spaces. Standard QRPA by default only provides *photoabsorption* strength functions; we extend the benchmark to finite-temperature QRPA (FT-QRPA), which is arguably the simplest possible extension of QRPA that offers access to the *photoemission* strength function and that has been used to study the LEE [19].

This paper is organized as follows: We remind the reader of the basics of both theoretical approaches in Sec. II. We present the results for the nuclear ground states and photoabsorption strength in Sec. III and discuss the origins of the discrepancies between the many-body methods. In Sec. IV we discuss the description of the photoemission strength in SM and FT-QRPA, including the temperature behavior of the computed strength functions and with an emphasis on the LEE. Finally, Sec. V concerns our conclusions and perspective for future developments aimed at the systematic microscopic description of magnetic dipole strength functions.

II. THEORY FRAMEWORK

In order to compare the results of different theoretical approaches we will discuss the sum rules, centroids, and widths

of strength distributions following the standard definitions [23,43]. Denoting the ground state and all the excited states by $|0\rangle$ and $|\nu\rangle$, respectively, the total strength,

$$S_0 = \sum_{\nu} |\langle \nu | \hat{O} | 0 \rangle|^2, \quad (1)$$

is the non-energy-weighted sum rule associated with a transition operator \hat{O} . The centroid and width of this strength function are then

$$\bar{S} = \frac{S_1}{S_0}, \quad \Delta S = \sqrt{\frac{S_2}{S_0} - \bar{S}^2}, \quad (2)$$

where

$$S_k = \sum_{\nu} (E_{\nu} - E_0)^k |\langle \nu | \hat{O} | 0 \rangle|^2 \quad (3)$$

is the (energy-weighted) sum rule of the order k . We focus here on the magnetic dipole operator:

$$\hat{O}(M1) = \sqrt{\frac{3}{4\pi}} \sum_k (g_l(k)\hat{l}(k) + g_s(k)\hat{s}(k))\mu_N, \quad (4)$$

where \hat{l} and \hat{s} are the orbital and spin angular momentum operators and the sum runs over all individual nucleons. The orbital and spin gyromagnetic factors are given by $g_l = 1$ and $g_s = 5.586$ for protons and $g_l = 0$ and $g_s = -3.826$ for neutrons. We employ these bare values for the orbital angular momentum but multiply the spin factors by 0.75 as customary for calculations limited to a valence space, see, e.g., Ref. [44] and references therein.

The reduced transition probability from an initial state $|i\rangle$ to a final state $|f\rangle$ is calculated as

$$B_{fi} = \frac{1}{2J_i + 1} \langle f | | \hat{O} | | i \rangle^2. \quad (5)$$

The $B(M1)$ distributions are convoluted with Lorentzians of an arbitrary width $2\gamma = 1$ MeV and converted into photostrength function (in units of MeV^{-3}) according to the formula [45]

$$f_{M1} = 16\pi/27(\hbar c)^3 \sum_f B_{fi}(M1) \frac{1}{\pi} \frac{\gamma}{(E - \Delta E_{fi})^2 + \gamma^2} \quad (6)$$

which leads to the continuous strengths presented in Figs. 3–7 and 9.

A. Model-space and Hamiltonian

Calculations are carried out using model spaces with well-established empirical interactions that are capable of describing (with a full diagonalization) the low-energy levels of nuclei within the major shell with an accuracy of around 200 keV: USDb [46] for the $1s0d$ shell, LNPS [47] for the $1p0f$ shell, and GCN5082 interaction [48,49] in the $0g_{7/2}1d_{2s_{1/2}}0h_{11/2}$ shell. Those shell-model interactions were proven to give a good agreement with experimental data in hundreds of studies of various observables, including those that depend on spin-isospin parts of the Hamiltonian, see, e.g., Refs. [50–53]. In particular, the analysis of 48 magnetic moments, 101 $M1$ and 232 Gamow-Teller matrix elements for

the USD family of the interactions was presented in Ref. [54], showing little dependence of those observables on the selected Hamiltonian and a good consistency with data. We emphasize that all shell-model studies known to us consistently indicate a low-energy enhancement of the $M1$ -dipole strength functions, of magnitude compatible with experimental evidence, and this independently on the details of valence space and effective Hamiltonian; see the discussion in Ref. [18].

For the purpose of this study we perform full-model space diagonalizations of the chosen Hamiltonians. As such diagonalizations become quickly difficult/impossible with the number of valence particles in the $0g_{7/2}1d_{2s_{1/2}}0h_{11/2}$ model space, only a few nuclei close to the $N = Z$ line and close to the $N = 82$ shell closure are considered (roughly the same nuclei for which the radiative decay was previously studied within the shell-model framework in Ref. [55]). The same quenching factor of 0.75 is applied on the spin part of the magnetic operator in all model spaces, even though more sophisticated prescriptions exist for a better agreement with experiment (see, e.g., Ref. [56]). However, the choice of effective operators does not play any role in this study aiming only in comparison of many-body methods.

B. Exact diagonalization

The reference results in this work are obtained in the shell-model framework, i.e., by diagonalization of the Hamiltonian in the basis of many-body states that can be constructed by placing n nucleons in the valence-space orbitals. We will dub those results hereafter as exact or shell-model results. Distributions of $B(M1)$ strengths in the shell model are computed using Lanczos strength functions method which permits to get the strength per energy interval in an efficient way [44]. We remind that the choice of the starting vector, called pivot, used in the Lanczos diagonalization procedure is arbitrary. Given a transition operator \hat{O} one can define a pivot of the form $\hat{O}|\Psi_i\rangle$, where $|\Psi_i\rangle$ can be chosen any shell-model state, and carry on Lanczos diagonalization. The unitary matrix U_{ij} that diagonalizes the Hamiltonian after N Lanczos iterations contains then in its first row the amplitude of the pivot in the j th eigenstate. Thus U_{1j}^2 as function of eigenenergies E_j defines the strength function of the pivot state. Note that to obtain the total strength S_0 for the ground state to be compared to QRPA only diagonalization of the 0^+ state has to be carried out in even-even nuclei, as the sum rule is the norm of the pivot state obtained by acting with the transition operator on the initial state. The remaining moments of the distribution presented in tables are extracted from the peaked-fence distributions obtained with the Lanczos strength function method with 100 iterations. These calculations are done using the m -scheme shell-model code ANTOINE [44,57]. In addition to photoabsorption strength, the decay strength functions are also computed employing the Bartholomew definition [58], following Refs. [12,18]:

$$f_{M1}(E_{\gamma}, E_i, J_i, \pi) = 16\pi/9(\hbar c)^3 \langle B(M1) \rangle_{\rho}(E_i, J_i, \pi), \quad (7)$$

where $\rho_i(E_i, J_i, \pi)$ is the partial level density determined at a given initial excitation energy E_i and $\langle B(M1) \rangle$ averaged reduced transition probability per energy bin. As such a

calculation requires computation of hundreds of converged excited states, the j -coupled code NATHAN [44] is employed to achieve this task and avoid numerical problems appearing in the m -scheme where large number of Lanczos iterations is necessary [44]. The details about energy and spin cutoffs of these calculations are given in Sec. IV for each of considered nuclei.

C. QRPA at zero and finite temperature

FT-QRPA builds on top of finite temperature Hartree-Fock Bogoliubov (FT-HFB) calculations where a mean-field pure Bogoliubov state is replaced by a statistical mixture of such states that minimizes the free energy subject to a particle-number constraint [59]. The resulting mixture is fully determined by (i) a Bogoliubov transformation that defines a set of quasiparticle operators $\{\beta, \beta^\dagger\}$ in terms of the single-particle operators $\{c, c^\dagger\}$,

$$\begin{pmatrix} \beta \\ \beta^\dagger \end{pmatrix} = \begin{pmatrix} U & V^* \\ V & U^* \end{pmatrix}^\dagger \begin{pmatrix} c \\ c^\dagger \end{pmatrix}, \quad (8)$$

and (ii) occupation numbers f related to the quasiparticle energies E_μ by

$$f_\mu \equiv \frac{1}{1 + e^{\frac{E_\mu}{k_B T}}}. \quad (9)$$

The generalized density matrix is diagonal in the quasiparticle basis and is entirely specified by the occupation numbers:

$$\mathcal{R}_0 = \begin{pmatrix} f & 0 \\ 0 & 1 - f \end{pmatrix}. \quad (10)$$

Taking a FT-HFB mixture as a reference point, FT-QRPA proceeds to define excitation modes Γ_μ^\dagger parametrized by finite temperature amplitudes $X^\mu, Y^\mu, P^\mu, Q^\mu$ as

$$\Gamma_\mu^\dagger \equiv \frac{1}{2} \sum_{ij} (P_{ij}^\mu \beta_i^\dagger \beta_j + X_{ij}^\mu \beta_i^\dagger \beta_j^\dagger - Y_{ij}^\mu \beta_j \beta_i - Q_{ij}^\mu \beta_j \beta_i^\dagger). \quad (11)$$

These amplitudes are obtained as solution of an eigenvalue equation that results from a linearization of either the time-dependent-FT-HFB equations [60] or the equation of motion [61,62].

FT-QRPA contains two different approximations that will make it deviate from the exact diagonalization:

- (i) The limitation of Eq. (11) to two-quasiparticle-excitations, preventing in particular explicit p-n correlations and restoration of symmetries broken by the mean-field reference state,
- (ii) the quasiboson approximation that is used in the derivation of the eigenvalue equation to evaluate nested commutators, thereby violating the Pauli exclusion principle [61].

The susceptibility of a nucleus with respect to a one-body transition operator F^1 , χ_F is defined as

$$\chi_F(\omega) \equiv \langle [\Gamma(\omega), F] \rangle_T, \quad (12)$$

where $\Gamma(\omega) \equiv \sum_\mu \frac{\Gamma_\mu}{\omega - \Omega_\mu}$, Ω_μ are the FT-QRPA poles and the notation $\langle \rangle_T$ indicates a thermal trace over the statistical mixture of HFB states. As a function of the susceptibility, the FT-QRPA excitation strength function becomes

$$S_F(\omega) \equiv -\frac{1}{\pi(1 - e^{-\beta\omega})} \text{Im} \chi_F(\omega). \quad (13)$$

This strength contains both an absorption ($\omega > 0$) and a de-excitation part ($\omega < 0$) that will be considered when studying the LEE.

Zero-temperature QRPA is naturally obtained as a limiting case of FT-QRPA, where all f identically vanish along with the P^μ and Q^μ amplitudes. This also means that the dimensionality of FT-QRPA is twice as large as that of QRPA. In practice, only single-particle states close to the Fermi energy are unblocked at low temperature, which tends to enrich the QRPA strength at low energies via the apparition of low-lying poles. The zero-T limit of Eq. (13) only retains transitions from ground to excited states while the thermal prefactor becomes a step function by making the deexcitation part vanish identically. In the rest of this work, zero-T QRPA is referred to as QRPA.

In the present work, we employ the recent numerical implementation of the finite amplitude method (FAM) for solving FT-QRPA equations. FT-QRPA-FAM replaces the intensive calculation and diagonalization of the FT-QRPA matrix by a set of nonlinear equations of similar dimension to that of the static Hartree-Fock-Bogoliubov mean-field approach it builds upon. The QRPA-FAM, first proposed in Refs. [63,64], has proven to be a very efficient tool to obtain electric [65,66] and charge-exchange [67,68] strength functions, as well as to determine collective inertia [69], quasiparticle-vibration coupling [70], discrete eigenmodes [71], and sum rules [72]. In a recent work [21] a QRPA-FAM implementation to compute zero- and finite-temperature strength functions using *ab initio* interaction was presented. Here we use the same numerical implementation to study dipole strength functions but with shell-model Hamiltonians. In particular, the present QRPA-FAM implementation does not impose axial symmetry and allows for reference states with triaxial deformation as we discuss in Sec. III D.

Axially symmetric QRPA-FAM calculations have been benchmarked with numerical implementation of the matrixial FT-QRPA formalism presented in Ref. [60] to the HF-SHELL code published in Ref. [59]. The results of both implementations match up to numerical precision. The results at (finite T) zero T will be indifferently referred to as (FT-)QRPA calculations in the following. Only even-even nuclei are computed in this work with FT-QRPA, an extension to odd systems is envisioned.

¹In the case of $M1$ transition, $F \equiv M^{1\mu}$.

III. GROUND STATES: ABSORPTION STRENGTH

We use a set of 25 spherical and deformed nuclei which can be described in the $1s0d$, $1p0f$, and $0g_{7/2}1d_{2s_{1/2}}0h_{11/2}$ spaces within the shell-model approach by exact diagonalization in the full model space. The same orbital spaces with their respective effective Hamiltonians are then used to perform calculations of transition strengths within the QRPA framework.

A. Mean-field solutions

The starting point of all (FT-) QRPA calculations is a mean-field state: We construct either (i) the HFB state that minimizes the total energy at zero temperature or (ii) the statistical mixture of HFB states that minimizes the free energy at finite temperature [59]. These configurations are constructed from single-particle states of definite proton or neutron nature expanded in the basis of the valence space orbitals, i.e., we do not allow for isospin mixing between protons and neutrons. We allow for the spontaneous breaking of rotational and particle number symmetry but restrict ourselves to axial symmetry except when explicitly mentioned. We summarize the results of our zero-temperature HFB calculations in Table I: We list ground-state energies from the exact diagonalization (E_{SM}) and the difference with respect to the HFB states (ΔE). To gauge the degree of symmetry breaking present in our mean-field configurations, we also include the quadrupole deformation β_{20} and whether the neutrons or protons form a pair condensate at the mean-field level.²

As can be seen from the table, the results for the ground-state energy fall into two groups: of light nuclei (sd -shell and pf -shell) where the disagreement is large and of the heavier nuclei ($gdsh$ -shell) where difference between exact and HFB energies is smaller, especially when compared to the total binding energy. In most cases, particle number and rotational symmetry are not simultaneously broken. If the former symmetry is not spontaneously broken, then the HFB formalism reduces in practice to the Hartree-Fock (HF) formalism while QRPA reduces to RPA.³ In what follows, we will use QRPA indiscriminately in all cases except when explicitly mentioned.

²The values of β_{20} we list should not be compared to values extracted from experimental data. The values we present reflect only the deformation of the valence nucleons, while intrinsic quadrupole deformation is a collective phenomenon that naturally includes contributions from all nucleons. We did not include a rescaling of the quadrupole operator to account for this effect here for simplicity.

³When pairing vanishes, QRPA reduces to the combination of RPA and PP-RPA: the first dealing with 1p-1h excitations and the second with 2p and 2h excitations [23]. We ignore this subtlety here, since the matrix element of the $M1$ operator between two Slater determinants with different particle number vanishes and hence does not contribute to strength functions. In general, however, the zero-pairing limit of HFB and QRPA approaches should be treated with care [73,74].

TABLE I. Ground-state properties of the nuclei considered in this study, organized by the corresponding valence space. We list minus the binding energy E_{SM} obtained with exact diagonalization (in MeV) and the energy difference with respect to (zero-temperature) HFB calculations $\Delta E \equiv E_{\text{SM}} - E_{\text{HFB}}$ (in MeV) as well as the quadrupole deformation β_{20} . The last two columns indicate whether pairing correlations are present in the HFB solution for each nucleon species (Y = yes, N = no).

Nucleus	E_{SM}	ΔE	β_{20}	E_p	E_n
²⁰ Ne	-40.47	-4.07	0.30	N	N
²⁴ Ne	-71.72	-5.32	0.18	N	Y
²⁴ Mg	-87.10	-6.34	0.27	N	N
²⁸ Mg	-120.49	-4.87	0.18	N	N
²⁸ Si	-135.86	-5.84	-0.24	N	N
³² Si	-170.52	-4.18	-0.13	N	N
³² S	-182.44	-6.05	0.00	N	N
³⁶ Ar	-230.27	-3.61	-0.11	N	N
⁴⁴ Ti	-46.88	-3.65	0.12	N	N
⁵⁰ Ti	-108.68	-4.34	0.00	Y	N
⁴⁸ Cr	-98.72	-4.67	0.16	N	N
⁵² Cr	-142.88	-4.08	0.05	Y	N
⁵² Fe	-151.64	-6.51	0.12	N	N
⁵⁶ Fe	-195.40	-7.27	0.12	N	Y
⁵⁶ Ni	-205.92	-6.36	0.00	N	N
⁶⁰ Ni	-248.04	-6.64	0.00	N	Y
⁶⁴ Zn	-303.02	-6.81	-0.15	Y	N
⁶⁴ Ge	-310.84	-8.56	-0.15	N	N
¹⁰⁴ Te	-50.26	-2.23	0.05	N	N
¹⁰⁸ Te	-98.05	-2.68	0.07	N	Y
¹⁰⁸ Xe	-102.52	-4.09	0.08	Y	Y
¹²⁸ Te	-282.14	-2.53	0.03	Y	Y
¹³² Te	-309.51	-1.25	0.00	Y	Y
¹³⁴ Xe	-353.22	-2.08	-0.02	Y	Y
¹³⁶ Ba	-396.02	-2.61	-0.03	Y	Y

B. $M1$ dipole response

The characteristics of the $B(M1)$ distributions for all computed nuclei are plotted in Fig. 1 comparing shell model to the axially deformed QRPA calculations. The general trends are easy to note and independent on the model space/Hamiltonian employed. The total strengths [Fig. 1(a)] exhibit the same tendencies in both approaches and agree within 20% for the majority of nuclei. One of the largest discrepancies, well visible in Fig. 1 around $A = 100$, concerns the $N = Z$ ¹⁰⁸Xe nucleus, which was predicted in a previous shell-model study with the same interaction to be triaxially deformed with $\beta = 0.16$ and $\gamma = 24^\circ$ [49]. The QRPA is missing nearly twice the strength predicted in the shell model in this case. Interestingly, in the other triaxial nucleus, ²⁴Mg, the QRPA sum rule overshoots the shell-model value by 35%. Thus the triaxiality itself is not the reason behind the missing strength observed in ¹⁰⁸Xe. The symmetry-unrestricted calculations verifying the actual impact of nonaxiality on the strength distributions in these two nuclei are presented in Sec. III D.

While the total strength seems reasonably reproduced by QRPA with a few exceptions, the centroids are always shifted to lower energies than the SM ones and the QRPA

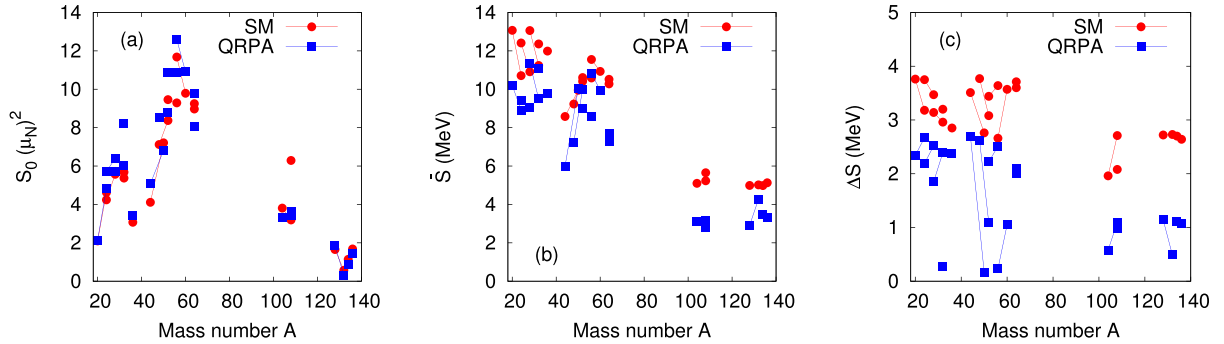


FIG. 1. Total strengths (a), centroids (b), and widths (c) for magnetic dipole operator as obtained in SM (red) and QRPA (blue) approaches for nuclei listed in Table I. The lines connect the same Z numbers.

distributions are less spread. This appears to be a common feature of the QRPA method for all transition operators as one can conclude comparing our results and those of Ref. [43]. One can also note that the width of the strength distributions are worse reproduced in spherical nuclei. While the small fragmentation of QRPA strengths can be attributed to the lack of higher-order particle-hole correlations, the shift of the centroid is more troublesome and additionally does not seem correlated with quadrupole deformation. The authors of Ref. [43] suspected inclusion of pairing within HFB + QRPA would improve the situation: As can be taken from our results, pairing correlations are not sufficient to cure the general shift of the QRPA distributions to lower energies. One can note from Fig. 1 that the behavior of centroids and widths is also the same in all studied regions, while only in the heaviest nuclei truly paired HFB mean-field solutions are obtained. The influence of pairing is, however, addressed in more detail in Sec. III C where the solutions with/without pairing correlations in selected nuclei are discussed.

The second hypothesis addressed in Ref. [43] was that the missing low-energy strength is due to the incomplete restoration of the symmetries in the RPA. For quadrupole strength, that is naturally impacted by rotational properties of the nucleus, the argument is indeed very well plausible and confirmed by other studies [75]. However, we suspect this does not hold for $M1$ transitions that are not expected to be of rotational character.

A possible explanation of the regular shift of the centroid towards lower energies can be traced back to the correlations missing in the mean-field treatments of ground and excited states. In Ref. [21] the effect of introducing correlations beyond HF + RPA on $E1$ photoabsorption cross sections was discussed with *ab initio* interactions. It was shown that introducing correlations to the ground state via coupled-cluster RPA or in-medium RPA leads to shifting of the whole strength in ^{16}O by 5 to 6 MeV providing a desired effect in view of our results. However, adding correlations also to the excited states through the second RPA method pushes the whole strength down by the same amount, resulting in photoabsorption cross section closer to the initial HF + RPA result. To get more insight into the correlations present in different approaches, we have computed occupations of the spherical orbits resulting the HF(B) calculations of the ground states for selected nuclei where the disagreement with the shell-model diagonalization

is particularly large. Those are compared to occupations from exact diagonalization in Table II. Since we consider $N = Z$ nuclei and the interactions are isospin conserving, the proton and neutron occupations are equal thus only one of them is reported in the table. We have also truncated shell-model calculations in order to get similar occupations as in HF(B)—those are indicated in the table as SM^{mod}. Further, we recomputed the $M1$ sum rules on such modified ground-state wave functions and used them as pivots in the Lanczos strength function method. The values of total strengths, centroids and widths obtained with such modified shell-model wave functions are given in Table III together with QRPA and full-space diagonalization results.

Taking first as examples spherical nuclei ^{32}S and ^{56}Ni , the HF wave functions are simply the lowest-filling configurations without correlations which are present in the shell-model solutions as seen from the table and the QRPA reduces to RPA in this case. We have thus truncated the SM configuration space to force the 0^+ states to be $0p$ - $0h$ configurations with respect to the reference Slater determinant and then allowed

TABLE II. Occupation of spherical orbits resulting the HF(B) calculations, exact diagonalization (SM), and truncated SM calculations (SM^{mod}) in selected $N = Z$ nuclei. See text for further details.

Nucleus	orbital	HF(B)	SM	SM ^{mod}
^{32}S	$0d_{5/2}$	6	5.48	6
	$1s_{1/2}$	2	1.45	2
^{56}Ni	$0d_{3/2}$	0	1.06	0
	$0f_{7/2}$	8	6.98	8
	$1p_{3/2}$	0	0.46	0
	$0f_{5/2}$	0	0.48	0
^{104}Te	$1p_{1/2}$	0	0.07	0
	$0g_{7/2}$	0.45	0.53	0.41
	$1d_{5/2}$	0.95	0.90	1.02
	$2s_{1/2}$	0.36	0.29	0.36
	$1d_{3/2}$	0.24	0.16	0.21
^{108}Xe	$0h_{11/2}$	0.0	0.12	0.0
	$0g_{7/2}$	1.40	1.37	1.31
	$1d_{5/2}$	1.58	1.49	1.67
	$2s_{1/2}$	0.55	0.53	0.64
	$1d_{3/2}$	0.39	0.31	0.38
	$0h_{11/2}$	0.08	0.30	0.0

TABLE III. Properties of the $M1$ strength distributions obtained in QRPA and SM and with modified SM wave functions of the ground state; see text for further details.

Nucleus		QRPA	SM	SM ^{mod}
³² S	S_0	8.21	5.68	10.55
	\bar{S}	11.07	12.36	11.41
	ΔS	0.27	3.20	0.30
⁵⁶ Ni	S_0	12.59	11.68	15.06
	\bar{S}	10.82	11.58	10.99
	ΔS	0.23	2.66	0.24
¹⁰⁴ Te	S_0	3.31	3.81	3.27
	\bar{S}	3.09	5.10	4.03
	ΔS	0.58	1.96	0.95
¹⁰⁸ Xe	S_0	3.64	6.29	4.91
	\bar{S}	3.15	5.65	4.12
	ΔS	0.98	2.08	1.43

for maximally 1p-1h excitations to the remaining orbits for both protons and neutrons to describe excited 1^+ states. A comparison of the shell-model $M1$ strength obtained in full and truncated model space is shown in Fig. 2, together with the RPA results, while the values characterizing these distributions are given in Table III. As can be seen, in ³²S the $M1$ strength in RPA calculations is concentrated in a single peak at 11.1 MeV with three other states predicted by the theory that carry very little strength. The diagonalization also gives four states at similar energies, with one major peak at 11.4 MeV. As one can see in the table, the diagonalization predicts, however, larger total strength but the centroid and

width are very close to the RPA values. Similarly, in ⁵⁶Ni the RPA gives two peaks, the one at 10.82 MeV carrying 99% of the $M1$ strength, in a good agreement with the restricted-space diagonalization, though the total strength is larger in the latter. Since the ground-state correlations and particle-hole content of excited states is now the same, the remaining difference between SM^{mod}+(1p-1h) and RPA most likely comes from the quasiboson approximation [23].

Contrary to the spherical nuclei ³²S and ⁵⁶Ni, in ¹⁰⁴Te the HF solution is much closer to that of the diagonalization though the $0h_{11/2}$ orbital remains empty in HF while 0.1 particle is occupying this orbital in the SM. The diagonalization performed preventing the particles to be promoted to the $0h_{11/2}$ orbital gives very similar occupations to the HF solution, see Table II, one can thus suppose the ground-state correlations are equally taken into account in the RPA and the SM^{mod}. Performing strength function calculations without any further restriction on the structure of excited states one recovers the total RPA strength in ¹⁰⁴Te; see Table III. Still, the centroid and width of the distribution with a modified ground state are between the RPA and full SM values meaning the approximations made in the RPA to describe excited phonon states are insufficient. Adding more nucleons in ¹⁰⁸Xe nontrivial pairing solutions are obtained in the ground state resulting in occupation of the $0h_{11/2}$ orbital of 0.08 particle versus 0.3 particle in the exact wave function. Repeating the exercise for ¹⁰⁸Xe to get similar orbital occupancy in SM and HFB ground states, the total strength from the exact solution goes lower without populating the $0h_{11/2}$ and thus gets closer to the QRPA value. The conclusions remain, however, the same as in ¹⁰⁴Te, in spite of pairing interactions additionally taken into account this time. These calculations evidence the crucial role of the *simultaneous* inclusion of correlations in ground and excited states to reproduce the centroid and width of the distribution. They also show (for the first two studied cases) that the quasiboson approximation introduces an additional inaccuracy to the calculation of the QRPA strength.

C. Role of pairing correlations

Since our selection contains many $N = Z$ nuclei, a remark about proton-neutron pairing correlations is in order. Those are not taken explicitly into account in the mean-field calculations which constitutes a difference with respect to the SM diagonalization. The role of $T = 1$ and $T = 0$ pairing interactions on rotational properties of lightest Xe nuclei with GCN5082 interaction employed here was previously discussed within the shell model in Ref. [49]. The deuteron-like $J = 1$ isoscalar pairs were shown to have a negligible presence in these nuclei and removing the $T = 0$ pairing interaction did not affect the quadrupole properties. In particular, the possibility of existence of the $T = 0$ pair condensate in the ground state of ¹⁰⁸Xe was refuted. The removal of isovector $T = 1$ pairing was shown to impact mostly the moment of inertia without considerably alternating of the decay properties of the band. Here we repeat the calculations from Ref. [49] to study the impact of p-n pairing interactions on $M1$ distributions in ¹⁰⁸Xe. To this end, a schematic pairing Hamiltonian was constructed with a strength adjusted to that of the GCN5082

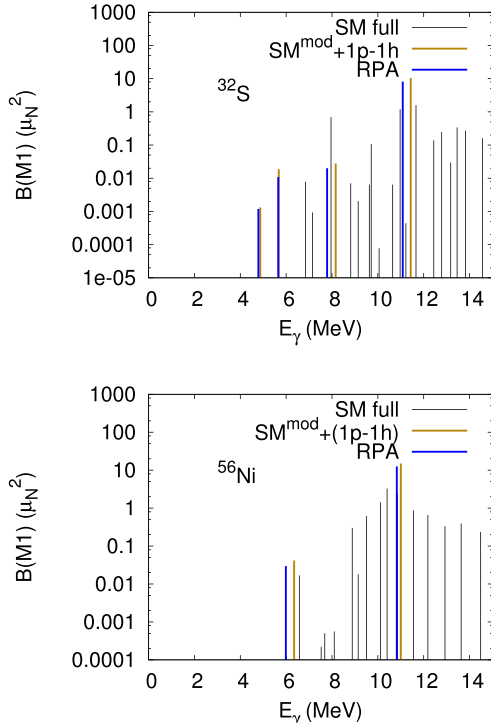


FIG. 2. $M1$ strength in RPA, SM, and modified SM calculations in ³²S and ⁵⁶Ni. See text for details.

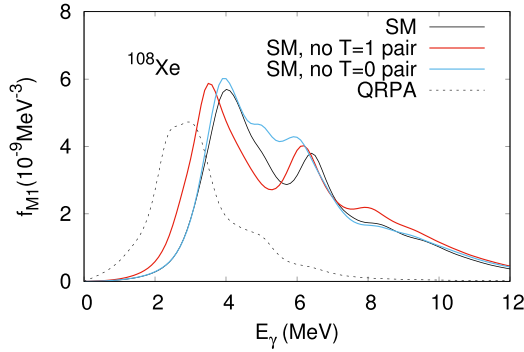


FIG. 3. $M1$ strength distributions of ^{108}Xe obtained by exact diagonalization with the full SM Hamiltonian (SM) and after removing schematic $T = 1$ (no $T = 1$ pair) and $T = 0$ (no $T = 0$ pair) interactions compared to the QRPA results. See text for details.

interaction on the two-body level. Further such a pairing Hamiltonian was subtracted from the interaction and the diagonalization of the 0^+ state carried out, followed by a calculation of the strength function. Figure 3 shows shell-model results with the full GCN5082 Hamiltonian and after removal of the $T = 0$ and $T = 1$ schematic pairing interactions. The $T = 0, J = 1$ proton-neutron pairing interaction does not play major role: The binding energy of the ground state is higher by 640 keV and the sum rule is enlarged by 8% without those correlations. The removal of the $T = 1, J = 0$ interactions has a bigger, though still limited impact, lowering the binding of the 0^+ by 900 keV and increasing the total strength by 11%. As can be seen in the figure, once convoluted with Lorentzians, the distributions look fairly similar: the whole distribution is shifted down when the $T = 1$ pairing is absent but the shape remains the same as in the full calculation. The absence of the $T = 0$ pairing produces no effect at the lowest energies but more strength is accumulated around 5 MeV. Overall, these effects are not significant enough to explain the difference with QRPA. The centroids of the three distributions agree within 100 keV and the widths within 300 keV. This little influence of pairing in the SM calculation of ^{108}Xe is not astonishing as its structure, similarly to the structure of many other nuclei along the $N = Z$ line, is dominated by quadrupole correlations in the shell-model picture. The proton-neutron pairing correlations in the $N = Z$ nuclei studied here are thus of minor importance, and one can suppose that taking them into account on the HFB level would not cure the rather important model differences.

Now let us turn back to the $T = 1$ pairing correlations and their role in the QRPA calculations. As said before, the results of Ref. [43] exhibited similar, systematic behaviors of the centroids and widths of the computed strength functions as we observe here for the magnetic dipole. This previous study was done within the RPA method only and thus pointed to the pairing correlations as possibly improving the results. To illustrate the effects of pairing in more detail, we have computed ^{60}Ni and ^{136}Ba nuclei using HF + RPA approach and compared to HFB + QRPA results, as depicted in Fig. 4. Clearly, the presence of pairing correlations is responsible for a shift of the strength of around 2 MeV in ^{136}Ba that is due

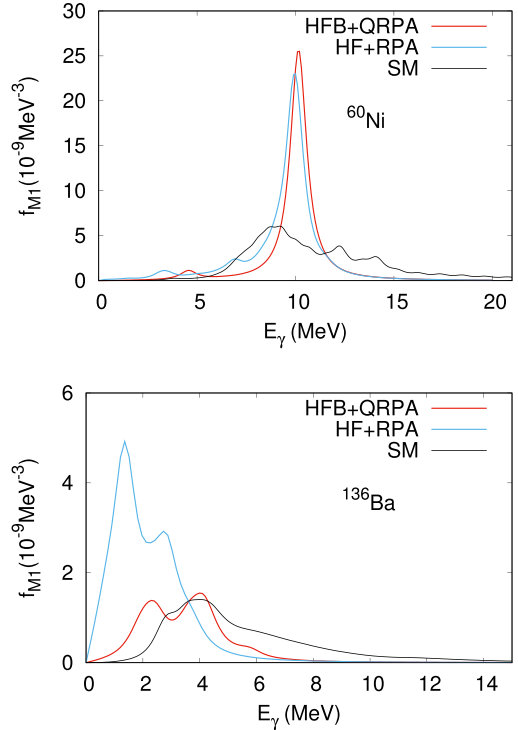


FIG. 4. Comparison of the HF + RPA, HFB + QRPA, and SM strengths in ^{60}Ni and ^{136}Ba .

to the lower energy of the HFB vacuum compared to the HF one. Pairing correlations also help with the spreading of the strength that turns out to be more fragmented. A shift of the centroid in the right direction is also observed in ^{60}Ni although less pronounced than in ^{136}Ba . This is probably explained by the fact that ^{60}Ni is only singly open-shell and only the neutrons are paired in the HFB calculation. These results suggest that symmetry-restored QRPA calculations [76] (in which the mean-field is expected to be more paired) might give results closer to SM.

D. Influence of triaxiality

In Fig. 5 the QRPA results obtained starting from the axially deformed and triaxial mean-field solutions are shown in both triaxial nuclei studied here, ^{24}Mg and ^{108}Xe . The changes due to triaxiality seem minor but go into the desired direction in both cases (note that the behavior of axial and nonaxial results is different in both nuclei): In ^{24}Mg the SM calculation gives $S_0 = 4.24\mu_N^2$, $\bar{S} = 12.41$ MeV, and $\Delta S = 3.75$ MeV. The QRPA calculation based on the axially deformed mean-field yields $S_0 = 5.72\mu_N^2$, $\bar{S} = 9.39$ MeV, and $\Delta S = 2.19$ MeV. As can be noted from the figure, the inclusion of nonaxiality in the ground state provides some reduction of the total strength ($S_0 = 4.96\mu_N^2$) and shifts the centroid to higher energies ($\bar{S} = 9.92$ MeV). There is, however, no broadening of the distribution. Contrary to ^{24}Mg , the total strength in ^{108}Xe is increased in the triaxial calculation from $S_0 = 3.64\mu_N^2$ to $S_0 = 4.87\mu_N^2$, bringing the solution to a slightly better agreement with the SM one: $S_0 = 6.29\mu_N^2$. The centroid shifts by 200 keV to the higher energy and is located

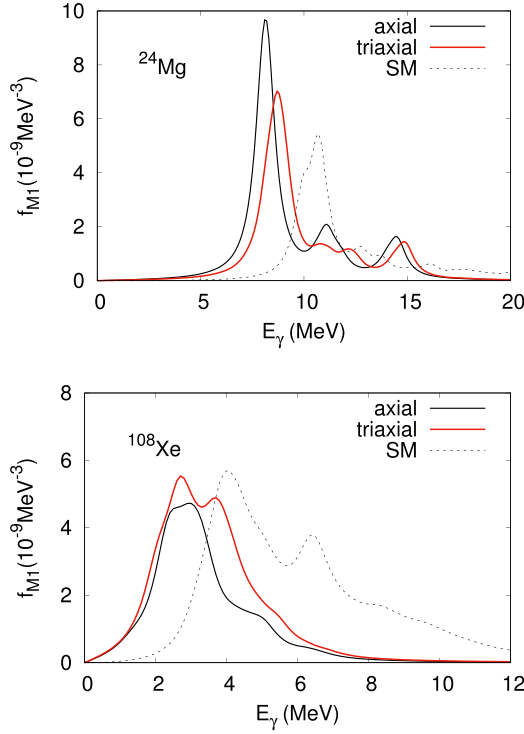


FIG. 5. Comparison of axially deformed and triaxial QRPA calculations to exact diagonalization for ^{24}Mg and ^{108}Xe nuclei.

at 3.34 MeV, still being too low with respect to the SM value of 5.65 MeV.

Similarly to what has been observed in Sec. III C, symmetry-breaking systematically goes in the direction of SM and further supports the idea that symmetry-restored QRPA might potentially help by favoring large symmetry breaking in the reference state and therefore improve prediction of $M1$ strength functions.

IV. EXCITED STATES: ABSORPTION AND EMISSION STRENGTH

Diverting our attention from the strength functions associated with the nuclear ground state, we turn to the $M1$ photoabsorption and photoemission strength at finite excitation energy, focusing on the origin of the LEE and whether it can be reproduced through QRPA calculations. We discuss first the photoabsorption and -emission strengths (and their difference) obtained from direct diagonalization, illustrating the presence of an LEE. We then extend our discussion to FT-QRPA: We compare exact and FT-QRPA results for both the absorption and emission strengths. To finish this section, we discuss future perspectives on the development of approaches that can account for this physical effect and yet avoid the computational cost of exact diagonalization.

A. Exact diagonalization: Absorption and emission

In Fig. 6, we compare the photoabsorption and emission strengths obtained from exact diagonalization in two heavy nuclei, ^{134}Xe (top panel) and ^{133}Xe (bottom panel). The

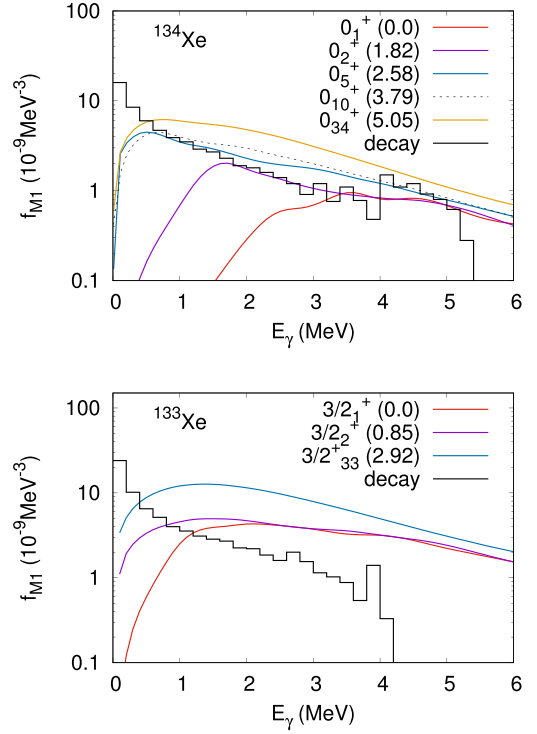


FIG. 6. Photoabsorption (colored, smooth lines) versus photoemission (black bins) strength functions obtained from exact diagonalization for ^{134}Xe (top panel) and ^{133}Xe (bottom panel). We label the photoabsorption curves with the quantum number and excitation energy (in parentheses, expressed in MeV) of the corresponding excited state.

figure includes the absorption strength for the ground state and several excited states, indicated by their quantum number and excitation energy. The decay strengths were computed by averaging transitions from many excited states using Eq. (7), including all excited states up to 6.0 MeV and $J = 7$ for ^{134}Xe and up to 4.0 MeV and $J = 15/2$. This selection included states of both parities for ^{133}Xe , but we limited ourselves to positive-parity states for the even-even nucleus for the sake of comparison to FT-QRPA results.

The LEE is clearly evident for ^{134}Xe : The deexcitation strength in the bin of lowest E_γ (0–0.2 MeV) is the largest across the entire energy range. The absorption strength of the nucleus grows with increasing excitation energy and approximates the decay strength across almost the entire range of the figure, except for the very lowest γ -ray energy bin. This figure illustrates the origin of the LEE as discussed in preceding shell-model studies: The LEE consists of low-energy γ transitions connecting the excited states in the quasicontinuum of nuclear levels. These conclusions are not significantly affected by our selection of states to compute the decay strengths [55]: (i) They are only weakly dependent on the considered spin and excitation energy range and (ii) negative-parity states in those nuclei contribute even more to the decay strength at low energy, leading to an even more pronounced LEE for ^{134}Xe , had we considered them. In fact, even restricting the calculation to 0^+ and 1^+ excited states still leads to similar shape and magnitude of the decay strength.

The deexcitation strength of the odd-even nucleus ^{133}Xe is qualitatively similar to that of ^{134}Xe , taking into account the 4-MeV cutoff in excitation energy in our calculation. There is a qualitative difference in the photoabsorption strengths, however: In contrast to the even-even nucleus, the odd-mass nucleus has significant strength for E_γ below 1 MeV even for the ground state. The origin of this difference is pairing: The low-energy spectrum of the even-even nucleus is much more sparse than that of its odd-mass neighbor, with the first 1^+ in ^{134}Xe at 2 MeV and the first excited state $1/2^+$ in ^{133}Xe at 0.25 MeV.

B. QRPA at finite temperature: Absorption

We first discuss the evolution of the $M1$ photoabsorption strength function with increasing excitation energy: Figure 7 shows the (FT-) QRPA strength functions for different values of the temperature in solid lines for one nucleus in each of the model spaces. We remind the reader that, as discussed in Sec. II C, the photoabsorption f_{M1} strengths are obtained from the positive-energy part of the FT-QRPA microscopic strength function S_{M1} . For each nucleus, an increase in temperature shifts the centroid to slightly lower γ -ray energies. The total strength obtained rises initially when increasing the temperature, but this trend reverses at the highest temperatures due to the limitations of the model space. Approaches based on energy density functionals are typically not limited to valence spaces: We anticipate that in such approaches the total strength will monotonously rise with increasing temperature.

Aside from these effects that affect the strength function as a function of temperature in a smooth way, there are discontinuous changes to be seen in the middle and bottom panels of Fig. 7. For ^{50}Ti , this is the development of two additional peaks, first near 5 MeV and at higher temperatures also near 2.5 MeV. For ^{134}Xe , the change in shape of the absorption strength is even more dramatic. In both cases, these changes reflect the discontinuous structural changes in the underlying mean-field solution that mark a temperature phase transition. These are illustrated in Fig. 8: The top panel shows the pairing phase transition in ^{50}Ti by means of the average proton pairing gap while the bottom panel shows the shape transition in ^{134}Xe by means of its quadrupole deformation β_{20} . ^{24}Mg also undergoes a phase transition from a prolate to a spherical shape, but for our model space and Hamiltonian this occurs for temperatures above those we consider here [59].

It is not trivial to compare FT-QRPA and SM results: The former depend on temperature and the latter on excitation energy. We relate the temperature of an excited 0^+ state to its excitation energy through a (phenomenological) model of the level density of the corresponding nucleus: $T = \sqrt{(E^* - \delta)/a}$ with E^* the calculated excitation energy, δ a pairing energy shift, and a the level density parameter. We use values of the latter two parameters from both the back-shifted Fermi gas and Gilbert-Cameron model as tabulated in Ref. [4], resulting in two temperatures for each excited SM state that we take as an indicative range. The resulting $M1$ strength functions obtained through exact diagonalization are drawn in Fig. 7 as dashed lines. The centroids of the SM $M1$ absorption strength for excited 0^+ states shift to energies that are several MeV

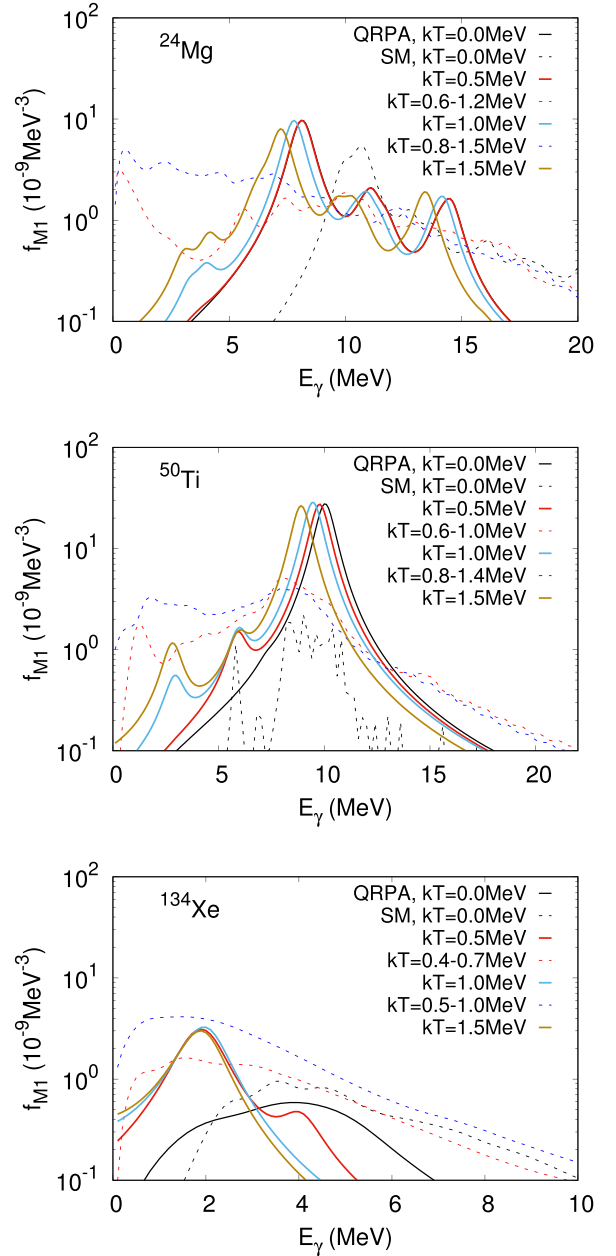


FIG. 7. The $M1$ photoresponse strength functions for ^{24}Mg (top), ^{50}Ti (middle), and ^{134}Xe (bottom) as obtained through FT-QRPA calculations for different values of the temperature (solid lines) and through exact diagonalization from initial states of different excitation energy (dashed lines).

lower than that of the ground state: many more 1^+ states find themselves in the direct vicinity of excited states. The total strength rises monotonously with temperature in this range of E_γ , although also the diagonalization approach will eventually face the limitations of the valence space at even higher excitation energies.

Comparing FT-QRPA and SM, we see a qualitative similarity in that the centroids shift to lower E_γ and that the total strengths increase with increasing excitation energy in both approaches. It is, however, immediately clear from all panels in Fig. 7 that these effects are too small in FT-QRPA:

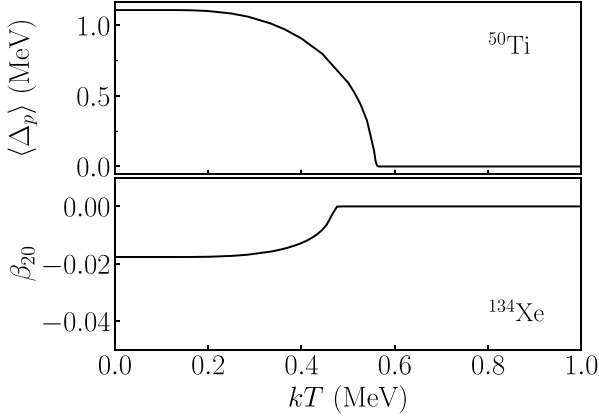


FIG. 8. Illustration of the temperature phase transitions for the FT-QRPA. Top panel: Average proton pairing gap in ^{50}Ti as a function of kT . Bottom panel: Quadrupole deformation β_{20} for ^{134}Xe .

The FT-QRPA absorption strength at high excitation energy differs dramatically from the exact result in all cases. This is in spite of the rather fair reproduction of the ground-state absorption strength for all three nuclei in Fig. 7, although the overall performance of FT-QRPA improves somewhat for heavier nuclei.

The reason for the failure of FT-QRPA is its level density: Because it is limited to two-quasiparticle excitations, the total number of many-body states that can be constructed is much smaller than those in an exact diagonalization. This is not so problematic when studying photoabsorption of the nuclear ground state, as many of the missing states are located at (comparatively) high excitation energy. Although the introduction of finite temperature allows for the construction of additional many-body states compared to a ground-state calculation (the thermal unblocking effect referred to in Sec. IIC), this does not suffice to capture the complexity of the entire many-body space. As an illustration, only 48 1p-1h excitations with $J^\pi = 1^+$ can be constructed for ^{24}Mg in the sd -shell while there are in total 3096 1^+ states that figure in an exact diagonalization.

Although our comparison is limited to even-even nuclei, we note that it is likely that FT-QRPA would compare somewhat better to the SM result for odd-mass and odd-odd nuclei. In those, the level density at low excitation energy is much higher as discussed in Sec. IVA such that FT-QRPA could possibly be able to capture a part of the absorption strength at low E_γ of the exact results.

C. QRPA at finite temperature: Deexcitation

In Fig. 9 we show the deexcitation strength function of ^{134}Xe obtained from SM and FT-QRPA calculations, the latter of which is derived from the microscopic strength function $S_{M1}(E)$ at negative energy as discussed in Sec. IIC.⁴ The evaluation of the SM strength

⁴We remind the reader that $S_{M1}(E)$ vanishes at negative energy at $kT = 0$: The formalism reduces to QRPA and the nuclear ground state cannot decay by emission of a photon.

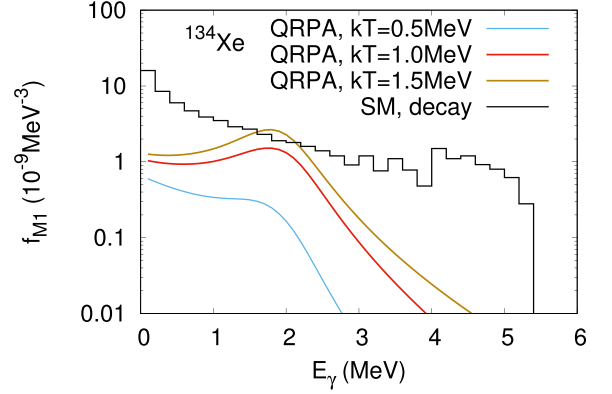


FIG. 9. Photoemission strength functions in ^{134}Xe obtained in the FT-QRPA approach versus the deexcitation strength function obtained from the shell-model diagonalization (see text for details).

included excited states up to ~ 6 MeV, which should correspond to a maximal temperature of $kT = 0.6$ – 1.1 MeV: We report FT-QRPA strength for a corresponding range of $kT = 0.5$ – 1.5 MeV.

Looking first at the FT-QRPA results by themselves, we see a significant evolution in the overall decay strength: As the temperature increases from $kT = 0.5$ to 1.5 MeV the total strength increases significantly across the range of E_γ .⁵ This increase is more rapid at higher E_γ , such that the centroid of the decay strength increases with increasing temperature. The nuclear susceptibility $\chi(\omega)$ depends on kT implicitly and carries most of the structural information of the mean-field configuration, but it varies very slowly with increasing temperature in the absence of phase transitions [77]. Most of the thermal evolution visible in Fig. 9 is due to the thermal prefactor in Eq. (13) which varies quickly with kT .⁶

Although some temperature enhancement is visible, the FT-QRPA strength at the lowest γ -ray energies differs from the SM result by roughly an order of magnitude even at high temperature. As the temperature increases, the level density accessible to FT-QRPA enlarges but this effect is not sufficient to produce an LEE that is comparable to the one obtained from exact diagonalization. Although some decay strength is produced at low energy, such strength is the tail of a peak located at roughly 2 MeV; this is a generic feature of even-even nuclei and it thus seems unlikely that FT-QRPA or other extensions of QRPA techniques that do not explicitly consider excited states would ever be able to produce a sufficiently large LEE. Similarly, approaches that obtain decay strength functions through photoabsorption strength functions of the ground states in even-even nuclei will likely fail to produce

⁵There is no discontinuous change due a phase transition visible on Fig. 9; the shape phase transition for ^{134}Xe is slightly below $kT = 0.5$ MeV.

⁶This thermal prefactor was not included in the study of dipole response based on *ab initio* Hamiltonians of Ref. [21]. The authors compared the susceptibility $\chi(\omega)$ with experimental data on the photodecay of ^{56}Fe .

the LEE, barring explicit inclusion through phenomenology. As discussed above, it is possible the situation is less dire for odd-mass and odd-odd nuclei where the level density at low energy is much higher.

As we mentioned above, the FT-QRPA is arguably the simplest extension of QRPA that directly results in decay strength functions. By virtue of the comparative simplicity of QRPA, FT-QRPA is likely the least numerically intensive many-body technique that provides such access. It is clear that this approach is, however, too simple to produce an LEE comparable to the SM result; one should look elsewhere for an approach that can cover the nuclear chart but still provide accurate dipole strength functions. There are multiple candidates for such an approach: A first is extending the QRPA framework with the calculation of all transitions between pairs of constructed states as opposed to just those rates involving the nuclear ground state [78]. Using the excitation energies and the reduced matrix elements obtained in this way, it should be possible to construct a decay strength function that probes a far larger level density although this has not yet been demonstrated at scale [79]. Multiphonon approaches constitute another path: These couple together multiple QRPA phonons and overcome some of the downsides of QRPA such as the fragmentation of the $M1$ strength [80,81] but have so far not been used to investigate the LEE due to $M1$ radiation. Although it has not been applied so far to describe dipole strength functions, the projected generator coordinate method (PGCM) is perhaps the most promising future avenue. PGCM has the potential to improve on (FT-) QRPA by (i) restoring quantum numbers lost by spontaneous symmetry breaking and hence enriching the nuclear ground state with additional correlations and (ii) capturing vibrational and rotational degrees of freedom within one single framework. Although this method scales modestly compared to exact diagonalization, polynomial as opposed to combinatorial, it remains demanding and has so far not been deployed at scale [82]. Finally, one could conceivably look for different computational techniques while keeping the power of SM results: shell model Monte Carlo (SMMC) techniques can provide exact results, up to statistical errors, in larger valence spaces than traditional diagonalization methods [83]. Reference [84] recently proved that one can use such techniques to study the LEE in rare-earth nuclei and it is plausible that even heavier nuclei could be addressed, though it is unlikely that systematic SMMC calculations will ever become feasible since the method remains bound to the construction of a valence space and effective interaction.

Although we conclude that standard (FT-) QRPA is not able to describe the LEE of magnetic dipole strength functions, we mention here that the method will likely fare better for the *electric* dipole strength function. SM calculations have shown that $1p-1h$ excitations typically suffice to describe low-energy $E1$ strength [12,85] while multiphonon approaches indicate that this strength can be captured by one-phonon calculations [86]. Because of this, we expect that most of the physically relevant part of the many-body space is accessible to (FT-) QRPA and the corresponding description of $E1$ transitions to be more successful. We will test this

expectation in a forthcoming study along the same lines as this one.

V. CONCLUSIONS

We have compared the absorption and decay magnetic dipole strength functions obtained from (FT-) QRPA and exact diagonalization in identical shell-model valence spaces and employing the same Hamiltonians. Our study spanned 25 even-even nuclei, from nuclei with $A \sim 28$ in the sd -shell up to medium-heavy nuclei with $A \sim 130$. Future work will be devoted to the study of electric dipole transitions along the same lines. The ground-state photoabsorption strength obtained from QRPA calculations is rather satisfactory: It typically agrees with the exact result within about 20%, although larger deviations occurred in our calculations. Other aspects of the (FT-) QRPA predictions are less appealing, and our results highlight two issues of this approach to obtain magnetic dipole strength functions.

The first issue concerns the lack of correlations in the nuclear ground state, which causes a systematic shift of the centroids of the $M1$ strengths towards lower γ -ray energies. We established that the size of this effect is somewhat lessened when the mean-field reference state incorporates more correlations through spontaneous symmetry breaking: Both the appearance of triaxial deformation and pairing condensate tend to improve the agreement with exact results, although we found proton-neutron pairing to be of very limited relevance. Nevertheless, it is unlikely that even the most general symmetry-broken configurations will be able to completely offset this effect, but our observation indicates that symmetry-restoration techniques are a promising route since they tend to drive the reference state towards less symmetrical configurations.

A second problem of the (FT-) QRPA is the truncation of many-body space to two-quasiparticle excitations on top of a mean-field reference state. This approximation leads to a level density that is too low, even at high excitation energies, leading to (i) a lack of fragmentation of the strength and (ii) a lack of strength at low E_γ for both photoabsorption and -decay strength functions of excited states. Most studies in the literature deal with the ground-state photoabsorption strength function of even-even nuclei; in this regime these deficiencies of QRPA are not immediately apparent since (i) a phenomenological smearing factor is incorporated to provide fragmentation and (ii) the sparsity of the low-energy spectrum of even-even nuclei forbids finite strength at low E_γ . The generalization of the formalism to finite temperature slightly enlarges the model space and allows for the appearance of some low-lying $M1$ strength, but the effect is typically far too small compared to the exact result. In particular, this indicates that traditional (FT-) QRPA approaches may not be reliable to predict the presence or absence of a low-energy enhancement of the $M1$ strength below the neutron emission threshold.

We cannot exclude that both drawbacks (lack of fragmentation and strength at low energy) can be partially remedied by incorporating $M1$ observables in parameter adjustments

of effective interactions or EDFs. We do not recommend this course of action though, as it seems unlikely that such a simple parameter renormalization would adequately capture these many-body effects. We discussed briefly alternative approaches to tackle this issue in a more systematic way that have a potential for global application; in particular, we mention that development of a framework to extract $M1$

strength functions from PGCM calculations based on shell-model Hamiltonians is underway [87].

ACKNOWLEDGMENTS

We gratefully acknowledge useful discussions with Sophie Péru. W.R. is a Research Associate of the F.R.S.-FNRS.

-
- [1] M. Arnould and S. Goriely, *Prog. Part. Nucl. Phys.* **112**, 103766 (2020).
- [2] H. Feshbach, C. Porter, and V. Weiskopf, *Phys. Rev.* **96**, 448 (1954).
- [3] Handbook for calculations of nuclear reaction data, RIPL.IAEA- TECDOC-1034, <http://www-nds.iaea.org/ripl/>.
- [4] <https://www-nds.iaea.org/RIPL-3/>.
- [5] <http://www.mn.uio.no/fysikk/>.
- [6] A. C. Larsen *et al.*, *Phys. Rev. Lett.* **111**, 242504 (2013).
- [7] H. Utsunomiya, S. Goriely, T. Kondo, C. Iwamoto, H. Akimune, T. Yamagata, H. Toyokawa, H. Harada, F. Kitatani, Y.-W. Lui *et al.*, *Phys. Rev. C* **88**, 015805 (2013).
- [8] A. Bürger *et al.*, *Phys. Rev. C* **85**, 064328 (2012).
- [9] A. C. Larsen *et al.*, *Phys. Rev. C* **85**, 014320 (2012).
- [10] A. C. Larsen and S. Goriely, *Phys. Rev. C* **82**, 014318 (2010).
- [11] R. Schwengner, S. Frauendorf, and A. C. Larsen, *Phys. Rev. Lett.* **111**, 232504 (2013).
- [12] K. Sieja, *Phys. Rev. Lett.* **119**, 052502 (2017).
- [13] R. Schwengner, S. Frauendorf, and B. A. Brown, *Phys. Rev. Lett.* **118**, 092502 (2017).
- [14] K. Sieja, *EPJ Web Conf.* **146**, 05004 (2017).
- [15] S. Karampagia, B. A. Brown, and V. Zelevinsky, *Phys. Rev. C* **95**, 024322 (2017).
- [16] S. Frauendorf, M. Beard, M. Mumpower, R. Schwengner, and K. Wimmer, *EPJ Web of Conferences* **93**, 04002 (2015).
- [17] S. Karampagia, B. A. Brown, and V. Zelevinsky, *J. Phys.: Conf. Ser.* **966**, 012031 (2018).
- [18] J. E. Midtbø, A. C. Larsen, T. Renstrøm, F. L. Bello Garrote, and E. Lima, *Phys. Rev. C* **98**, 064321 (2018).
- [19] E. Litvinova and N. Belov, *Phys. Rev. C* **88**, 031302 (2013).
- [20] H. Wibowo and E. Litvinova, *Phys. Rev. C* **100**, 024307 (2019).
- [21] Y. Beaujeault-Taudière, M. Frosini, J.-P. Ebran, T. Duguet, R. Roth, and V. Somà, *Phys. Rev. C* **107**, L021302 (2023).
- [22] B. A. Brown and A. C. Larsen, *Phys. Rev. Lett.* **113**, 252502 (2014).
- [23] P. Ring and P. Schuck, *The Nuclear Many-body Problem* (Springer-Verlag, Berlin, 1980).
- [24] N. Paar, D. Vretenar, E. Khan, and G. Colo, *Rep. Prog. Phys.* **70**, R02 (2007).
- [25] J. Terasaki and J. Engel, *Phys. Rev. C* **82**, 034326 (2010).
- [26] M. Martini, S. Péru, S. Hilaire, S. Goriely, and F. Lechaftois, *Phys. Rev. C* **94**, 014304 (2016).
- [27] G. Kruzić, T. Oishi, and N. Paar, *Phys. Rev. C* **103**, 054306 (2021).
- [28] D. Gambacurta, M. Grasso, V. De Donno, G. Co', and F. Catara, *Phys. Rev. C* **86**, 021304 (2012).
- [29] D. Gambacurta, M. Grasso, and J. Engel, *Phys. Rev. C* **92**, 034303 (2015).
- [30] F. Knapp, P. Papakonstantinou, P. Veselý, G. D. Gregorio, J. Herko, and N. L. Iudice, *Phys. Rev. C* **107**, 014305 (2023).
- [31] R. Trippel, Ph.D. thesis, Collective excitations with chiral NN+3N interactions from coupled-cluster and in-medium SRG, TU Darmstadt (2016).
- [32] V. Tselyaev, N. Lyutorovich, J. Speth, and P.-G. Reinhard, *Phys. Rev. C* **102**, 064319 (2020).
- [33] S. Goriely and E. Khan, *Nucl. Phys. A* **706**, 217 (2002).
- [34] S. Goriely, S. Hilaire, S. Péru, M. Martini, I. Deloncle, and F. Lechaftois, *Phys. Rev. C* **94**, 044306 (2016).
- [35] S. Goriely, S. Hilaire, S. Péru, and K. Sieja, *Phys. Rev. C* **98**, 014327 (2018).
- [36] L.-G. Cao, H. Sagawa, and G. Colò, *Phys. Rev. C* **83**, 034324 (2011).
- [37] M. Anguiano, G. Co', V. De Donno, and A. M. Lallena, *Phys. Rev. C* **83**, 064306 (2011).
- [38] P. Wen, L.-G. Cao, J. Margueron, and H. Sagawa, *Phys. Rev. C* **89**, 044311 (2014).
- [39] V. Tselyaev, N. Lyutorovich, J. Speth, P.-G. Reinhard, and D. Smirnov, *Phys. Rev. C* **99**, 064329 (2019).
- [40] G. Kruzić, T. Oishi, D. Vale, and N. Paar, *Phys. Rev. C* **102**, 044315 (2020).
- [41] S. Sun, L.-G. Cao, F.-S. Zhang, H. Sagawa, and G. Colò, *Phys. Rev. C* **109**, 014321 (2024).
- [42] K. Sieja and S. Goriely, *Eur. Phys. J. A* **57**, 110 (2021).
- [43] I. Stetcu and C. W. Johnson, *Phys. Rev. C* **67**, 044315 (2003).
- [44] E. Caurier, G. Martinez-Pinedo, F. Nowacki, A. Poves, and A. P. Zuker, *Rev. Mod. Phys.* **77**, 427 (2005).
- [45] H. Loens *et al.*, *Eur. Phys. J. A* **48**, 34 (2012).
- [46] B. A. Brown and W. A. Richter, *Phys. Rev. C* **74**, 034315 (2006).
- [47] S. M. Lenzi, F. Nowacki, A. Poves, and K. Sieja, *Phys. Rev. C* **82**, 054301 (2010).
- [48] A. Gniady, E. Caurier, F. Nowacki, and A. Poves (unpublished).
- [49] E. Caurier, F. Nowacki, A. Poves, and K. Sieja, *Phys. Rev. C* **82**, 064304 (2010).
- [50] W. A. Richter and B. A. Brown, *Phys. Rev. C* **80**, 034301 (2009).
- [51] C. Wraith, X. Yang, L. Xie, C. Babcock, J. Bieroń, J. Billowes, M. Bissell, K. Blaum, B. Cheal, L. Filippin *et al.*, *Phys. Lett. B* **771**, 385 (2017).
- [52] K. Sieja, G. Martinez-Pinedo, L. Coquard, and N. Pietralla, *Phys. Rev. C* **80**, 054311 (2009).
- [53] A. Mollaebrahimi, C. Hornung, T. Dickel, D. Amanbayev, G. Kripko-Koncz, W. R. Plaß, S. Ayet San Andrés, S. Beck, A. Blazhev, J. Bergmann *et al.*, *Phys. Lett. B* **839**, 137833 (2023).
- [54] W. A. Richter, S. Mkhize, and B. A. Brown, *Phys. Rev. C* **78**, 064302 (2008).
- [55] K. Sieja, *Phys. Rev. C* **98**, 064312 (2018).
- [56] G. Jakob, N. Benczer-Koller, G. Kumbartzki, J. Holden, T. J. Mertzimekis, K.-H. Speidel, R. Ernst, A. E. Stuchbery, A. Pakou, P. Maier-Komor *et al.*, *Phys. Rev. C* **65**, 024316 (2002).
- [57] E. Caurier and F. Nowacki, *Acta Phys. Pol. B* **30**, 705 (1999).

- [58] G. A. Bartholomew, E. D. Earle, A. J. Ferguson, J. W. Knowles, and M. A. Lone, in *Advances in Nuclear Physics*, edited by M. Baranger and E. Vogt (Springer, Boston, MA, 1973), Vol. 7, pp. 229–324.
- [59] W. Ryssens and Y. Alhassid, *Eur. Phys. J. A* **57**, 76 (2021).
- [60] W. Ryssens and Y. Alhassid, Solution of the finite-temperature (q)rpa equations for shell-model Hamiltonians: Hf-shell v2, (unpublished).
- [61] D. Rowe, *Nuclear Collective Motion* (Methuen & Co., London, 1970).
- [62] H. Sommermann, *Ann. Phys.* **151**, 163 (1983).
- [63] T. Nakatsukasa, T. Inakura, and K. Yabana, *Phys. Rev. C* **76**, 024318 (2007).
- [64] P. Avogadro and T. Nakatsukasa, *Phys. Rev. C* **84**, 014314 (2011).
- [65] T. Inakura, T. Nakatsukasa, and K. Yabana, *Phys. Rev. C* **80**, 044301 (2009).
- [66] M. Stoitsov, M. Kortelainen, T. Nakatsukasa, C. Losa, and W. Nazarewicz, *Phys. Rev. C* **84**, 041305 (2011).
- [67] E. M. Ney, J. Engel, T. Li, and N. Schunck, *Phys. Rev. C* **102**, 034326 (2020).
- [68] M. T. Mustonen, T. Shafer, Z. Zenginerler, and J. Engel, *Phys. Rev. C* **90**, 024308 (2014).
- [69] K. Washiyama, N. Hinohara, and T. Nakatsukasa, *Phys. Rev. C* **103**, 014306 (2021).
- [70] E. Litvinova and Y. Zhang, *Phys. Rev. C* **104**, 044303 (2021).
- [71] N. Hinohara, M. Kortelainen, and W. Nazarewicz, *Phys. Rev. C* **87**, 064309 (2013).
- [72] N. Hinohara, *Phys. Rev. C* **92**, 034321 (2015).
- [73] T. Duguet, B. Bally, and A. Tichai, *Phys. Rev. C* **102**, 054320 (2020).
- [74] T. Duguet and W. Ryssens, *Phys. Rev. C* **102**, 044328 (2020).
- [75] A. Porro, T. Duguet, J.-P. Ebran, M. Frosini, R. Roth, and V. Somà, *Ab initio* description of monopole resonances in light- and medium-mass nuclei iv. angular momentum projection and rotation-vibration coupling, (unpublished).
- [76] C. Federsmidt and P. Ring, *Nucl. Phys. A* **435**, 110 (1985).
- [77] E. Lipparini, *Modern many-particle physics: Atomic gases, Quantum Dots and Quantum Fluids* (World Scientific Publishing Company, Singapore, 2003).
- [78] S. Kamedzhiev and D. Voitenkov, [arXiv:1110.0654](https://arxiv.org/abs/1110.0654).
- [79] L. Gaodefroy, S. Péru, N. Arnal, J. Aupiais, J.-P. Delaroche, M. Girod, and J. Libert, *Phys. Rev. C* **97**, 064317 (2018).
- [80] N. Tsoneva and H. Lenske, *Phys. Rev. C* **77**, 024321 (2008).
- [81] G. Rusev, N. Tsoneva, F. Dönau, S. Frauendorf, R. Schwengner, A. P. Tonchev, A. S. Adekola, S. L. Hammond, J. H. Kelley, E. Kwan *et al.*, *Phys. Rev. Lett.* **110**, 022503 (2013).
- [82] T. Duguet, J.-P. Ebran, M. Frosini, H. Hergert, and V. Somà, *Eur. Phys. J. A* **59**, 13 (2023).
- [83] S. E. Koonin, D. J. Dean, and K. Langanke, *Phys. Rep.* **278**, 1 (1997).
- [84] P. Fanto and Y. Alhassid, *Phys. Rev. C* **109**, L031302 (2024).
- [85] Noritaka Shimizu, Takashi Abe, Michio Honma, Takaharu Otsuka, Yusuke Tsunoda, Yutaka Utsuno, and Tooru Yoshida, *JPS Conf. Proc.* **6**, 010021 (2015).
- [86] N. Tsoneva, H. Lenske, and C. Stoyanov, *Phys. Lett. B* **586**, 213 (2004).
- [87] S. Bofos, J. Martinez-Larraz, B. Bally, T. Duguet, M. Frosini, T. Rodriguez, and K. Sieja, Application of projected generator coordinate method for m1 strength function calculation in valence space (unpublished).